Supplementary material for ”Regional, multi-decadal analysis reveals that stream temperature increases faster than air temperature”

Hanieh Seyedhashemi et al.

Table S1. Vegetation species and their approximated height (extracted from: Otto (1998); Aulinger et al. (2005); Allaby (2019); https://cms.geobretagne.fr/; www.polebocage.fr).

Species	Height (m)
Wood forest	25
Coniferous forest	25
Deciduous forest	25
Open forest	20
Mixed forest	25
Poplar grove	25
Bocage	15
Mixed woody vegetation	20
Shrub	10
Grass	0

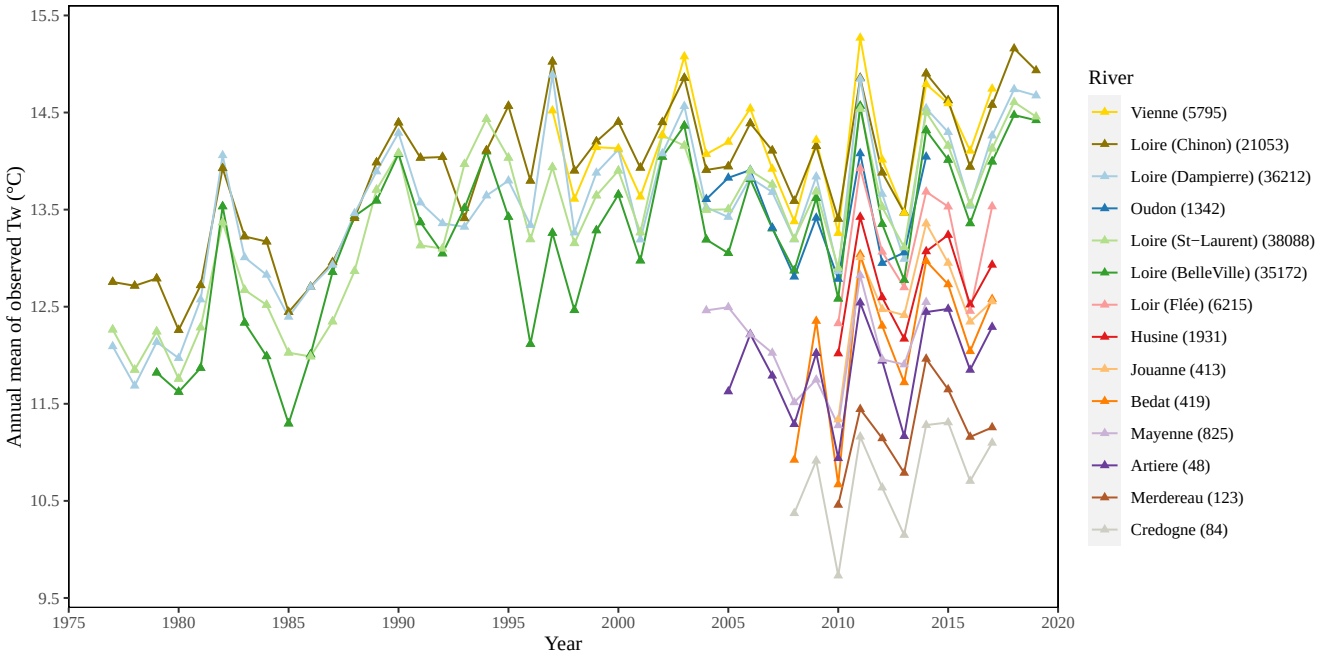

Figure S1. The annual mean of observed Tw at the 14 stations with long-term data between 1977 and 2019 (see Table 1). The numbers within the parentheses show the river catchment area (km^2).

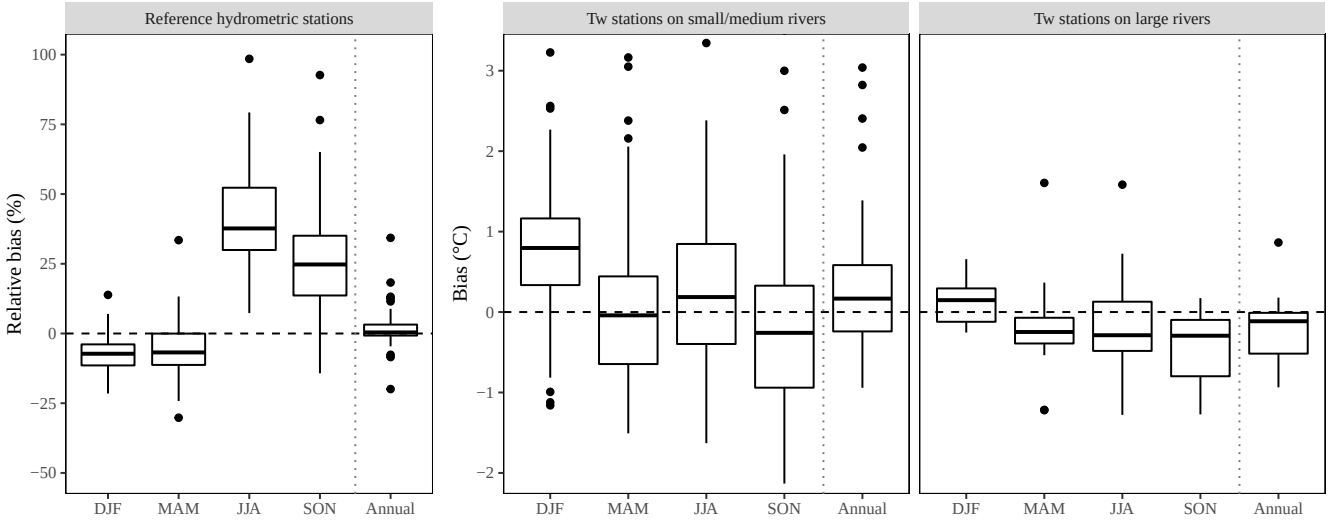

Figure S2. Relative bias of the EROS hydrological model at 44 stations from the Reference Hydrometric Network (RHN) over the 1968–2019 period (left). Absolute bias of the TNET thermal model at 72 observed Tw stations (58 on small and medium rivers, middle; 14 on large rivers, right) over the 2010–2014 period. Values for seasonal (DJF = winter; MAM = spring; JJA = summer; SON = autumn) and annual bias are presented separately.

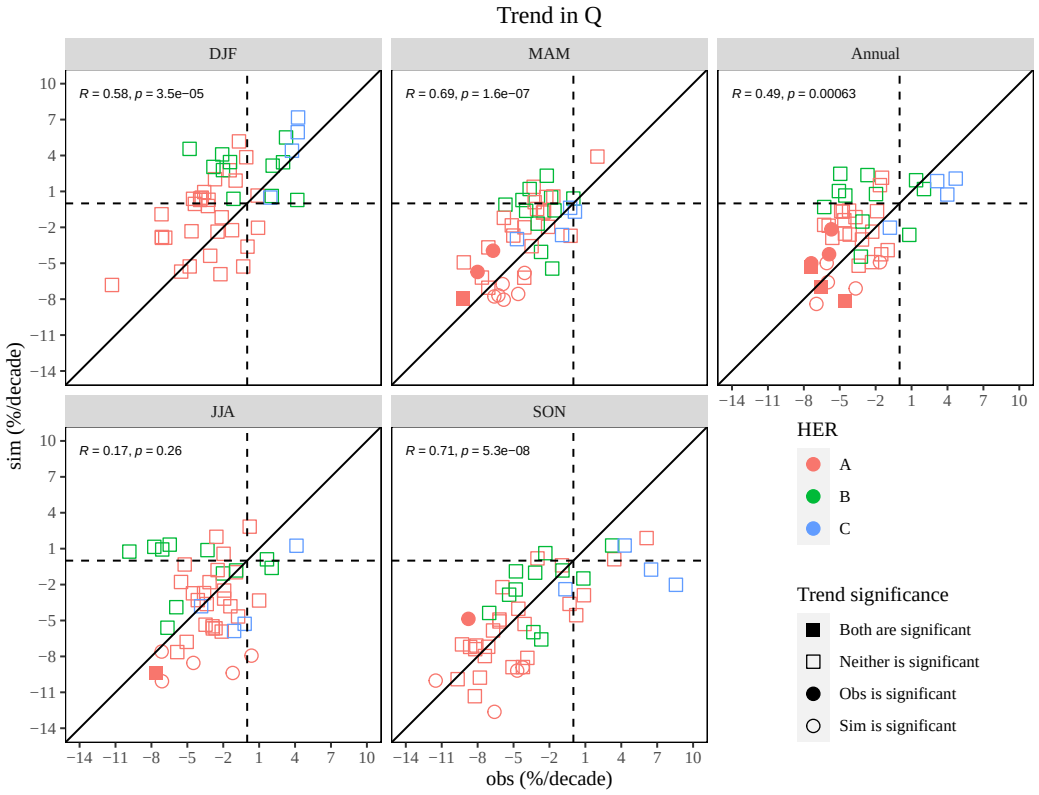

Figure S3. Relationships between long-term trends (1968–2019) in observed and simulated Q for 44 reference hydrometric stations, at the seasonal and annual scales. Point shapes indicate whether trends are significant or not at the 95% confidence level for observations and simulations according to the Mann-Kendall test. Colors refer to the Hydro-Ecoregion (HER) where the station is located (see Fig. 1).

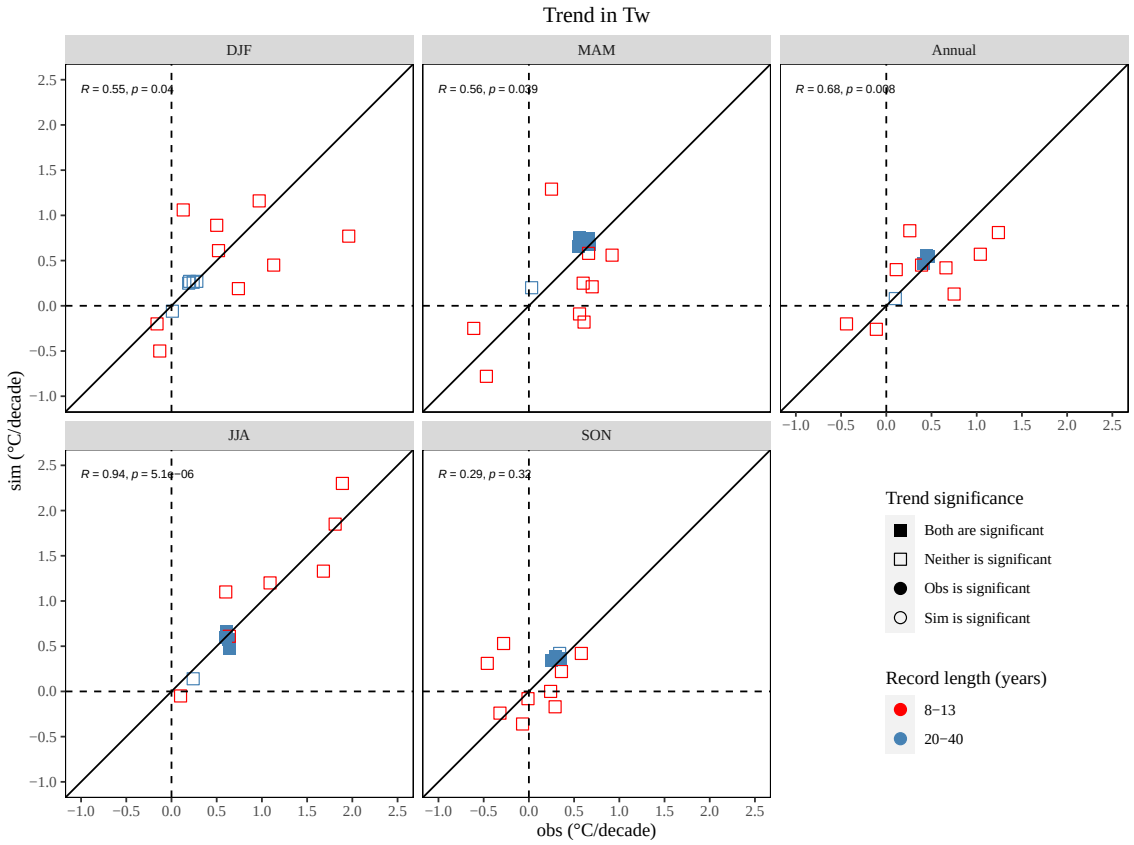

Figure S4. Relationships between trends in observed and simulated Tw for 14 stations, including 5 stations with long-term data (20-40 years, blue) and 9 stations with 8-13 years of data (red). Point shapes indicate whether trends are significant or not at the 95% confidence level for observations and simulations according to the Mann-Kendall test. The trends in observed and simulated Tw were either both significant or neither was significant. Colors refer to total number of years with data.

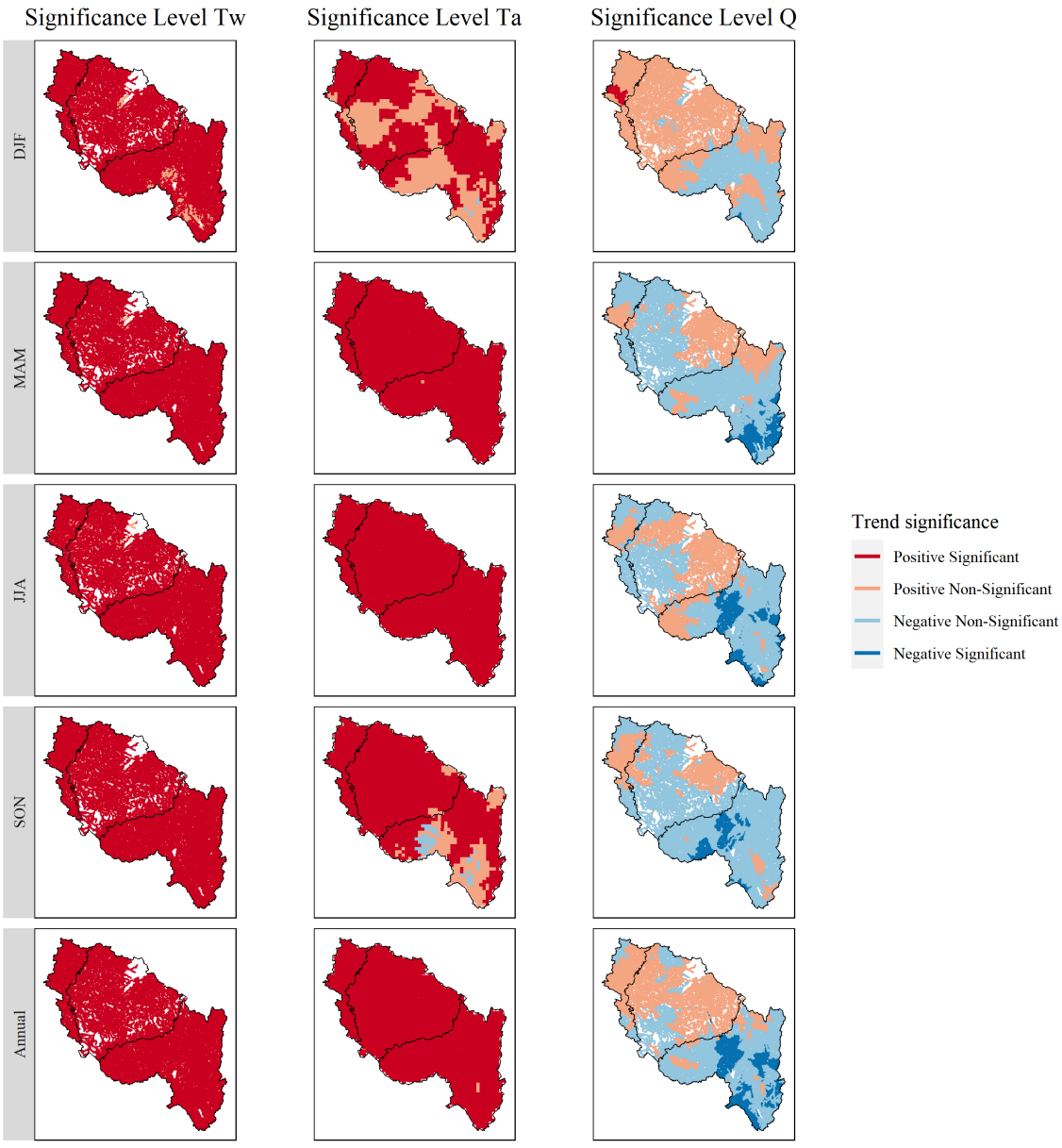

Figure S5. Spatial variability of the significance of trends in seasonal and annual Tw, Ta and Q over the 1963–2019 period, based on a Mann-Kendall test at the 95% confidence level. Solid black lines show the Hydro-Ecoregion delineation (see Fig. 1).

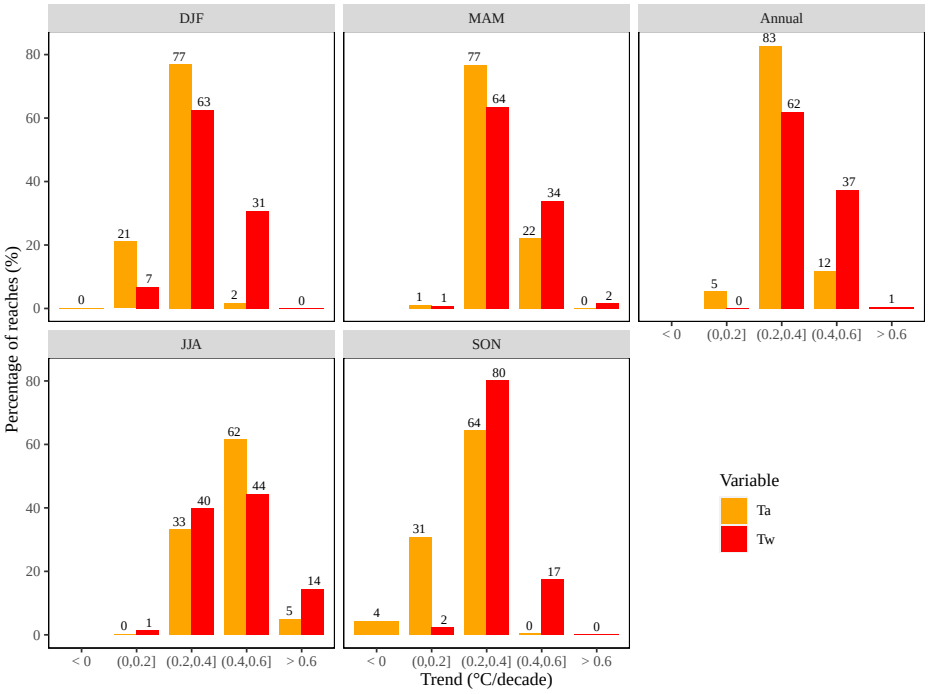

Figure S6. The range of the seasonal and annual Tw and Ta trends for all 52278 reaches over the 1963–2019 period. This representation includes both significant and non-significant trends.

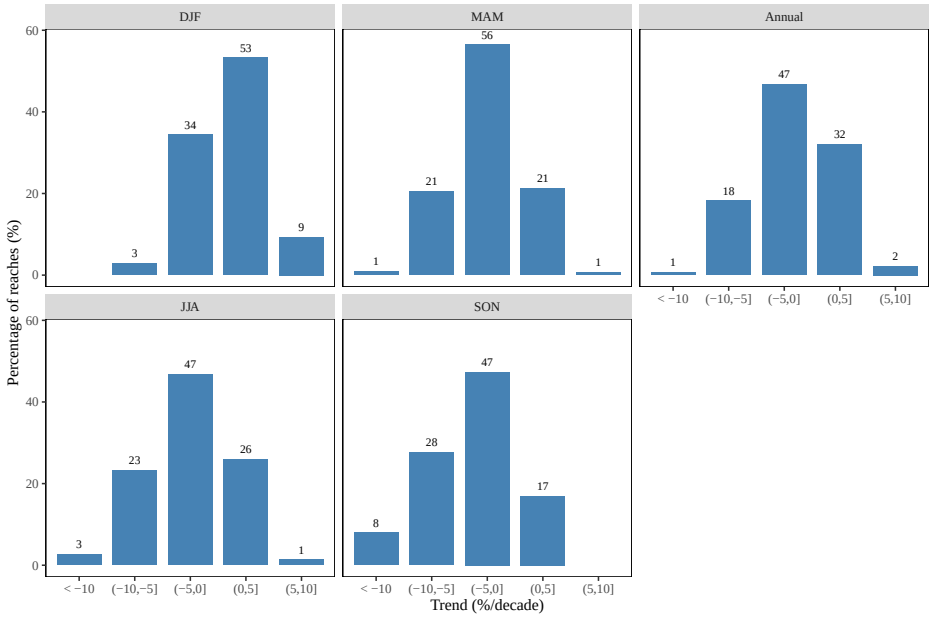

Figure S7. The range of the seasonal and annual Q trends for all 52278 reaches over the 1963–2019 period. This representation includes both significant and non-significant trends.

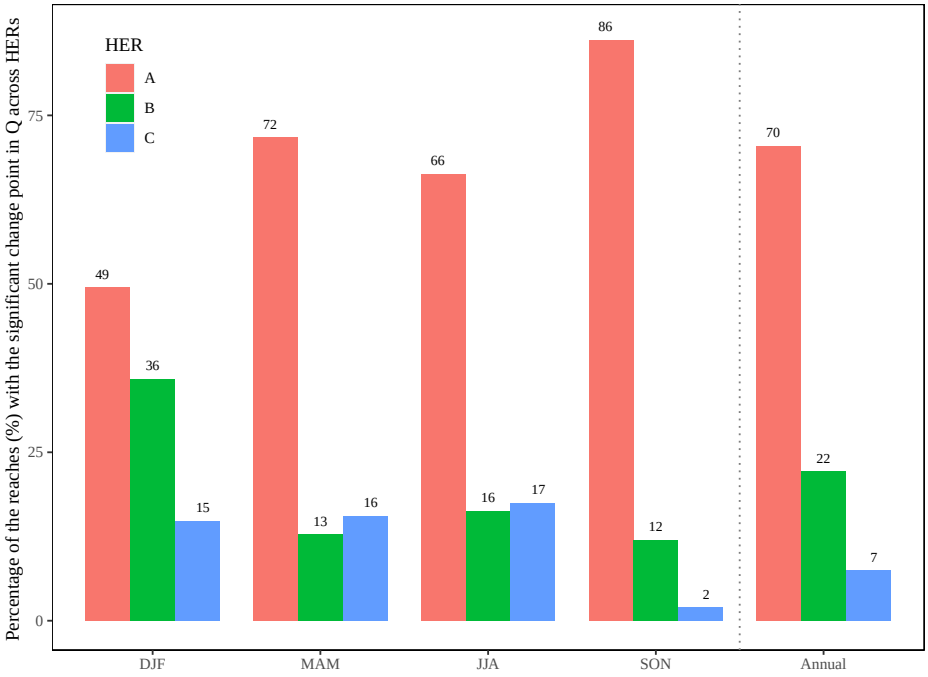

Figure S8. Percentage of reaches with the detected significant change-point in Q time series across HERs. Note that, in this figure, the percentage has been calculated over the reaches with the significant change-point, not over whole 52278 reaches.

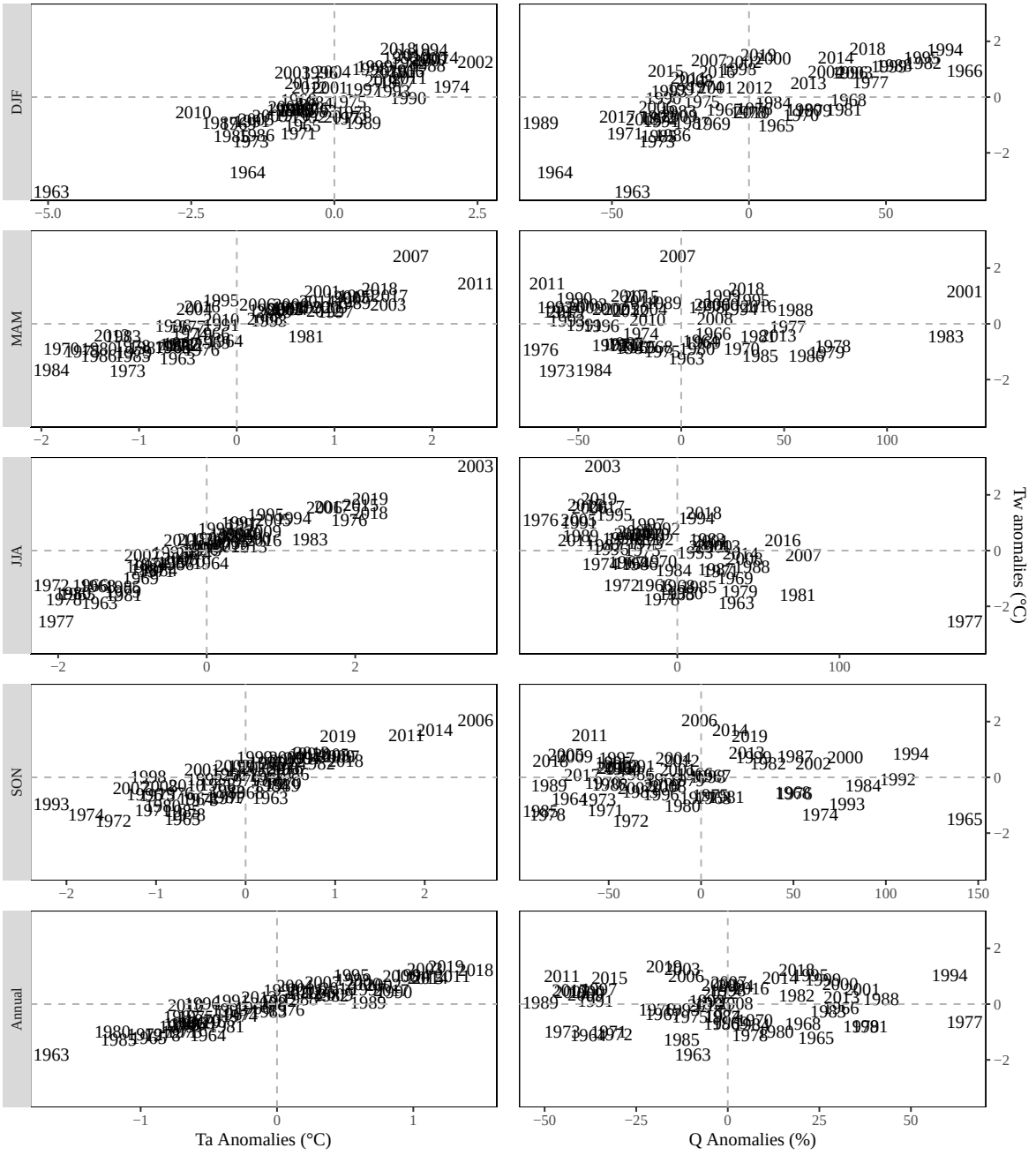

Figure S9. Synchronicity of Tw anomalies with Ta anomalies and Q anomalies at seasonal and annual scale. The labels indicate the median anomalies of 52278 reaches for each year.

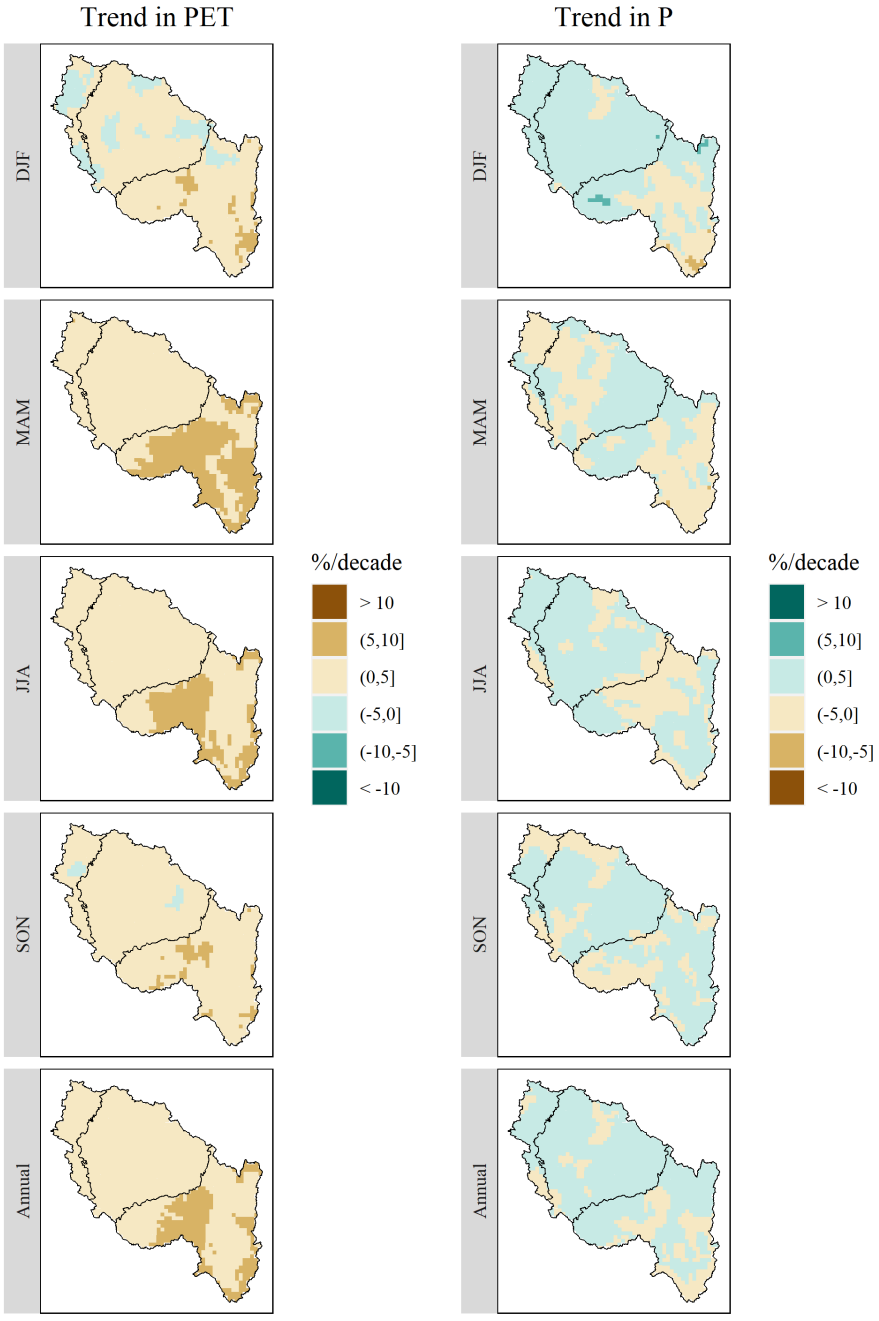

Figure S10. The spatial variability of trends in seasonal and annual potential evapotranspiration (PET) and total precipitation (P) over the 1963–2019 period. The solid black lines are showing the borders of HER (see Fig. 1).

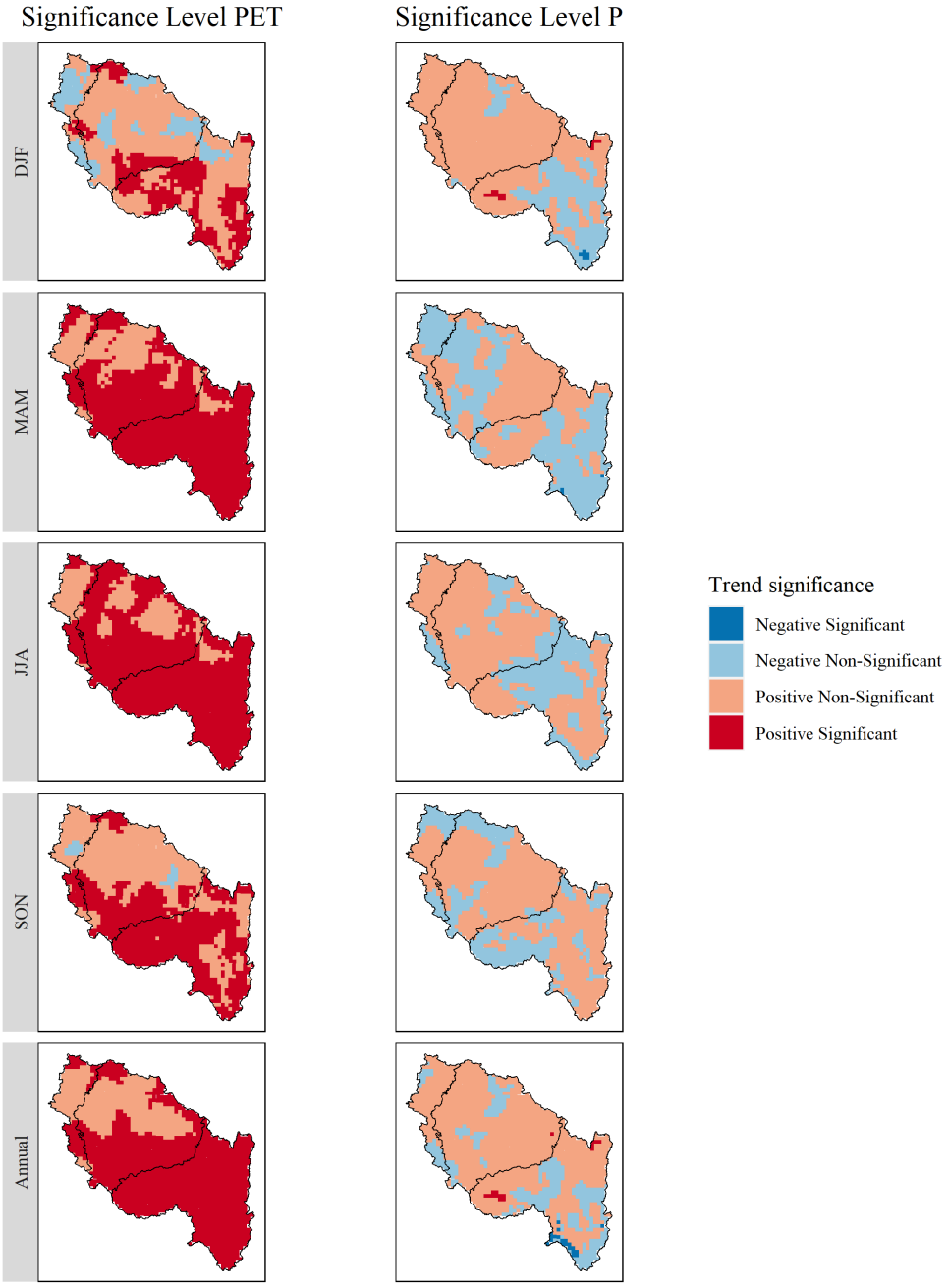

Figure S11. The spatial significance level of trends in seasonal and annual P and PET the 1963–2019 period. The solid black lines are showing the borders of HERs.

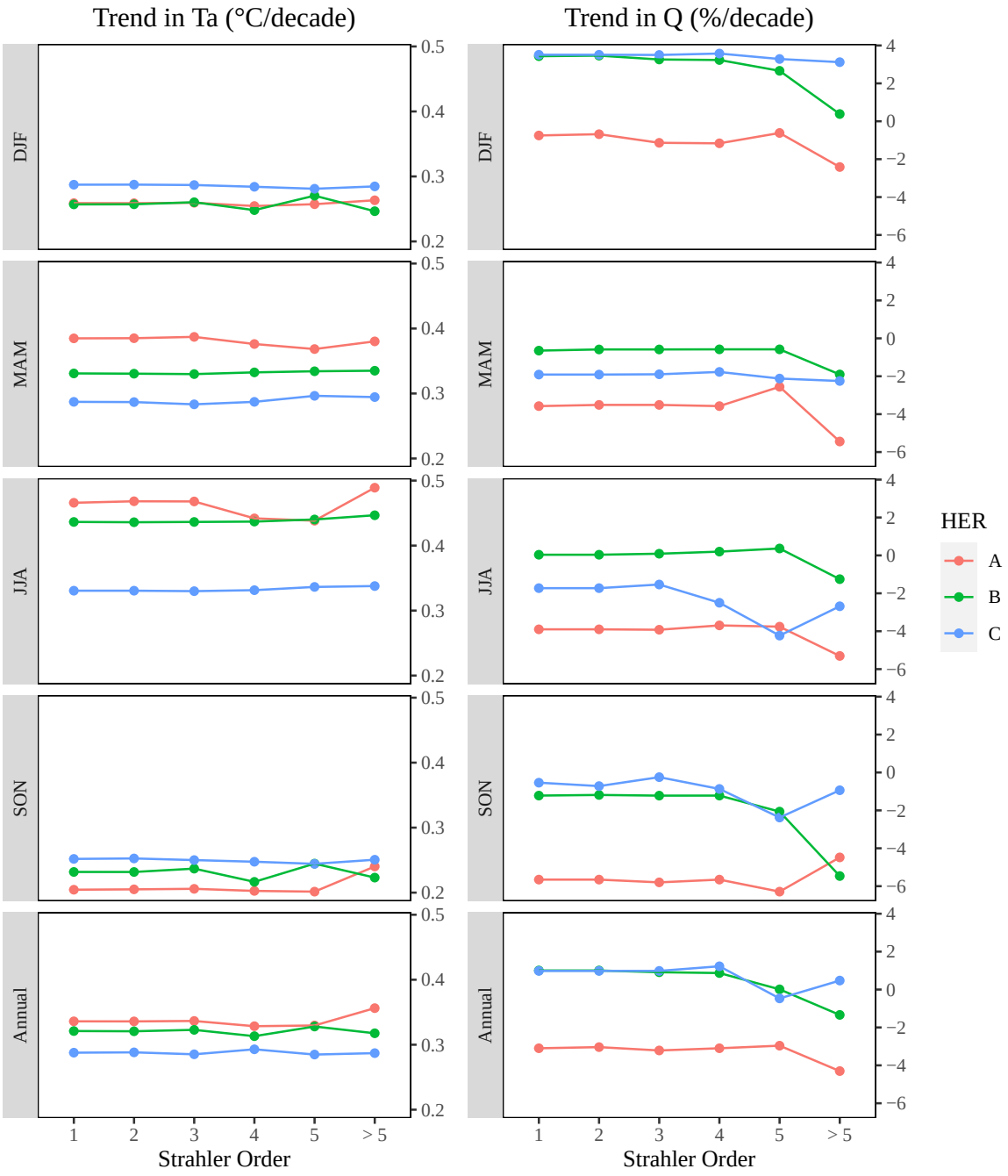

Figure S12. Relationships between median trends in Ta and Q over the period 1963—2019 and reach size (Strahler order; 1=small streams, >5=large rivers). The relationships are shown by HER and by season (DJF=winter; MAM=spring; JJA=summer; SON =fall).